inorganics

MDPI

Article

Synthesis, X-ray Structure, Hirshfeld Surface Analysis and Antimicrobial Assessment of Tetranuclear *s*-Triazine Hydrazine Schiff Base Ligand

Hessa H. Al-Rasheed [1,*], Sarah A. AL-khamis [1], Ayman El-Faham [2], Assem Barakat [1], Alexandra M. Z. Slawin [3], John Derek Woollins [3,4] and Saied M. Soliman [2,*]

[1] Department of Chemistry, College of Science, King Saud University, P.O. Box 2455, Riyadh 11451, Saudi Arabia; 441203438@student.ksu.edu.sa (S.A.A.-k.); ambarakat@ksu.edu.sa (A.B.)
[2] Department of Chemistry, Faculty of Science, Alexandria University, P.O. Box 426, Ibrahimia, Alexandria 21321, Egypt; ayman.elfaham@alexu.edu.eg or aymanel_faham@hotmail.com
[3] School of Chemistry, University of St Andrews, Andrews KY16 9ST, UK; amzs@st-andrews.ac.uk (A.M.Z.S.); jdw3@st-andrews.ac.uk (J.D.W.)
[4] Department of Chemistry, Khalifa University, Abu Dhabi 999041, United Arab Emirates
* Correspondence: halbahli@ksu.edu.sa (H.H.A.-R.); saied1soliman@yahoo.com or saeed.soliman@alexu.edu.eg (S.M.S.); Tel.: +20-1111361059 (S.M.S.)

Abstract: The unexpected tetranuclear $[Cu_4(DPPT)_2Cl_6]$ complex was obtained by self-assembly of $CuCl_2.2H_2O$ and (*E*)-2,4-di(piperidin-1-yl)-6-(2-(1-(pyridin-2-yl)ethylidene)hydrazinyl)-1,3,5-triazine, (**HDPPT**) in ethanol. In this tetranuclear $[Cu_4(DPPT)_2Cl_6]$ complex, the organic ligand acts as mononegative chelate bridging two crystallographically independent Cu(II) sites. The **DPPT**$^-$ anion acts as a bidentate ligand with respect to Cu(1), while it is a tridentate for Cu(2). The $Cu(1)N_2Cl_3$ and $Cu(2)N_3Cl$ spheres have square pyramidal and square planar coordination geometries with some distortion, respectively. Two of the chloride ions coordinating the Cu(1) are bridging between two crystallographically related Cu(1) sites connecting two $[Cu_2(DPPT)Cl_3]$ units together, leading to the tetranuclear formula $[Cu_4(DPPT)_2Cl_6]$. The packing of the $[Cu_4(DPPT)_2Cl_6]$ complex is dominated by C-H. . .Cl contacts, leading to one-dimensional hydrogen-bond polymeric structure. According to Hirshfeld surface analysis of molecular packing, the non-covalent interactions H. . .H, Cl. . .H, Cl. . .C, C. . .H, and N. . .H are the most significant. Their percentages are 52.8, 19.0, 3.2, 7.7, and 9.7%, respectively. Antimicrobial assessment showed good antifungal activity of the Cu(II) complex against *A. fumigatus* and *C. albicans* compared to Ketoconazole as positive control. Moreover, the $[Cu_4(DPPT)_2Cl_6]$ complex has higher activity against Gram-positive bacteria than *Gentamycin* as positive control. The opposite was observed when testing the tetranuclear $[Cu_4(DPPT)_2Cl_6]$ complex against the Gram-negative bacteria.

Keywords: tetranuclear; *s*-triazine; Cu(II); X-ray structure; Hirshfeld; antimicrobial activity

Citation: Al-Rasheed, H.H.; AL-khamis, S.A.; El-Faham, A.; Barakat, A.; Slawin, A.M.Z.; Woollins, J.D.; Soliman, S.M. Synthesis, X-ray Structure, Hirshfeld Surface Analysis and Antimicrobial Assessment of Tetranuclear *s*-Triazine Hydrazine Schiff Base Ligand. *Inorganics* **2023**, *11*, 357. https://doi.org/10.3390/inorganics11090357

Academic Editor: Moris S. Eisen

Received: 11 August 2023
Revised: 23 August 2023
Accepted: 28 August 2023
Published: 30 August 2023

1. Introduction

Supramolecular chemistry is concerned with the chemistry beyond the molecule. It focuses on the assembly of molecular systems via non-covalent interactions. Currently, Supramolecular chemistry is considered a well-accepted discipline in chemistry due to the diverse applications in different areas, such as gas absorption, nanoreactors, molecular sensors, chemical catalysis, drug delivery, and molecular machines [1]. Moreover, this field of chemistry has applications in maintenance-free materials [2,3], molecular encapsulation [4,5], and medical diagnostic sensors [6]. Hence, this growing branch of chemistry is found in a variety of daily uses where its applications extend to sensors, medicine, materials, and extraction technologies [7]. Coordination compounds attract the attention of scientists as a consequence of their wide range of applications in diverse fields [8–15]. Copper is an important metal in coordination chemistry as well as in

biology [16–19]. Its compounds are recommended as therapeutic agents for treatments of many diseases, including microbial infections [20–23], lung inflammation [24], influenza A [25], cancer [26], and others [27–30]. Copper has a high ability to form coordination compounds where its coordination environment is dependent on many factors, including its oxidation state, ligand nature, and medium used [31,32].

On the other hand, heterocyclic compounds are important organic compounds used in coordination chemistry as ligands to build interesting metal-organic systems [33–36]. Moreover, Schiff base compounds have great importance in coordination chemistry in addition to their diverse applications in different areas, including industrial food, chemosensors, polymer stabilizers catalysis transformation, pigments and dyes, and also as starting materials for synthesizing a wide range of biologically active compounds [37]. The introduction of heterocyclic moiety in a Schiff base derivative produces powerful chelating ligands with higher chelation capacity for the synthesis of metal-organic complexes. In this regard, the six-membered aromatic ring with alternating C and N-atoms, which is known as *s*-triazine, has attracted the attention of researchers in supramolecular chemistry for molecular assembly to construct interesting metal-organic architectures. Hence, many *s*-triazine chelating ligands were designed for the construction of metal complexes with fascinating applications and interesting biological activities [38].

Recently, our research group studied the coordination chemistry of some *s*-triazine Schiff base ligands, exploring their coordination chemistry towards different metal ions and showing their molecular and supramolecular characteristics (Scheme 1) [39–43]. Among these *s*-triazine Schiff base ligands, the 2,4-*bis*(morpholin-4-yl)-6-[(*E*)-2-[1-(pyridin-2-yl)ethylidene]hydrazin-1-yl]-1,3,5-triazine (**DMPT**) form a number of metal complexes with Ni(II), Cu(II), Cd(II), Zn(II), and Mn(II) metal salts. In all cases, the structure of the resulting complexes was approved using a single crystal X-ray structure to be monomeric and the ligand acting as a neutral tridentate *NNN*-chelate.

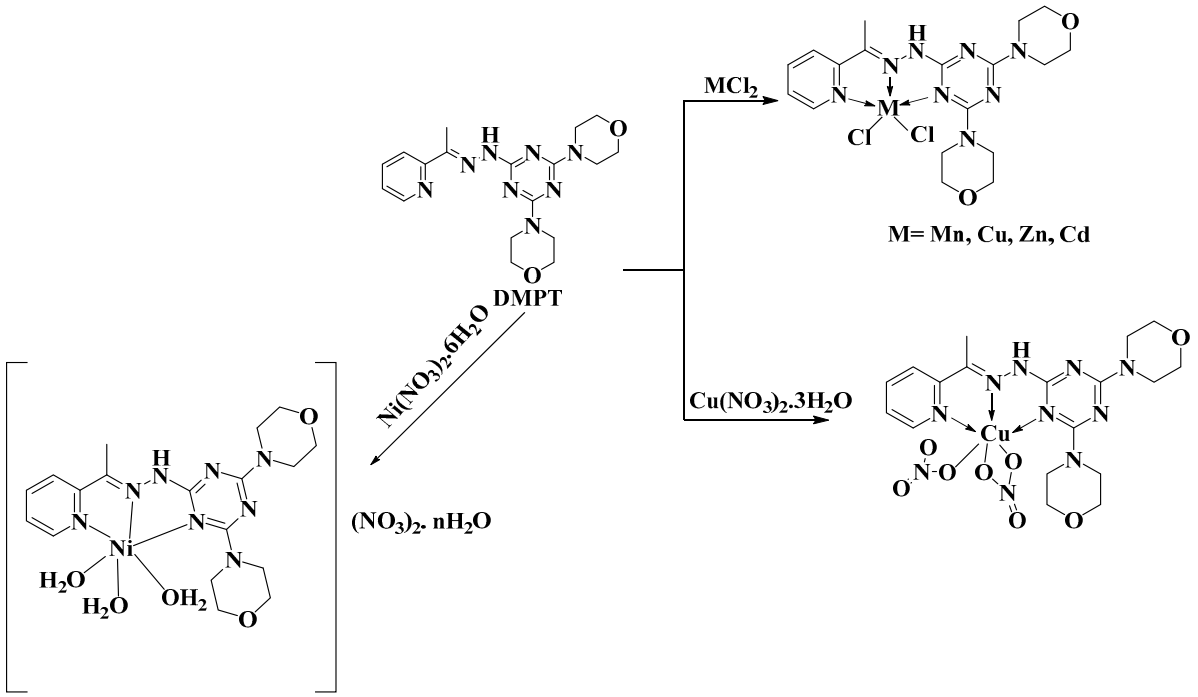

Scheme 1. Synthesis of the previously reported metal(II) complexes with 2,4-*bis*(morpholin-4-yl)-6-[(*E*)-2-[1-(pyridin-2-yl) ethylidene]hydrazin-1-yl]-1,3,5-triazine, (**DMPT**).

Furthermore, the *bis*-piperidino analog ((*E*)-2,4-di(piperidin-1-yl)-6-(2-(1-(pyridin-2-yl)ethylidene)hydrazinyl)-1,3,5-triazine, (**HDPPT**)) formed mononuclear complexes with Ni(II) and also behaved as a neutral tridentate *NNN*-chelate (Scheme 2) [41]. As a continuation of our previous studies on the *bis*-piperidino analog ligand, we tested the reaction of

this ligand with copper chloride dihydrate using the same reaction conditions. The resulting complex was isolated in good crystallinity, allowing the confirmation of the structure using single-crystal X-ray diffraction in addition to FTIR spectra and elemental analyses. In addition, the supramolecular structure of this complex was analyzed using Hirshfeld surface analysis. The activity of the synthesized complex against some harmful microbes is examined.

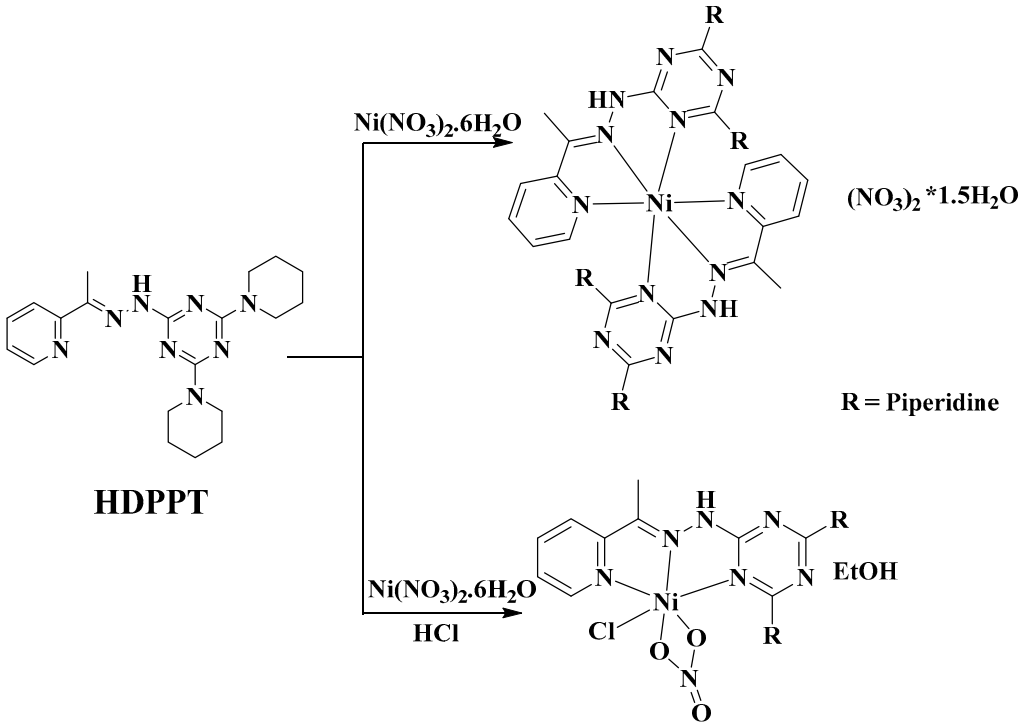

Scheme 2. Synthesis of the Ni(II)-**HDPPT** complexes.

2. Results and Discussion

2.1. Synthesis and Characterization

In our previous studies, the synthesis including X-ray structure characterization and antimicrobial activities of the self-assembled monomeric complexes $[Ni(HDPPT)_2](NO_3)_2$*$1.5H_2O$ and $[Ni(HDPPT)(NO_3)Cl]$.EtOH was presented. The two Ni(II) complexes were prepared by reaction of Ni(II) salts with HDPPT ligand in ethanol [41]. The HDPPT ligand acts as a neutral tridentate chelate in both cases. In this work, self-assembly of the HDPPT ligand and copper chloride dihydrate in ethanol afforded the tetranuclear $[Cu_4(DPPT)_2Cl_6]$ complex as dark green crystals after one week of slow evaporation at room temperature (Scheme 3). Unlike the corresponding $[Ni(HDPPT)_2](NO_3)_2$*$1.5H_2O$ and $[Ni(HDPPT)(NO_3)Cl]$.EtOH complexes of the same ligand, the NH proton of the ligand was deprotonated during the course of the reaction. Hence, the ligand in the case of the current Cu(II) complex is acting as a mononegative ligand but not a neutral one as found in the Ni(II) complexes. FTIR spectra of the $[Cu_4(DPPT)_2Cl_6]$ complex revealed the deprotonation of the HDPPT ligand. The $\nu_{(N\text{-}H)}$ vibration of the ligand was detected at 3279 cm^{-1}, this band completely disappeared in the $[Cu_4(DPPT)_2Cl_6]$ complex. Moreover, the $\nu_{(C=N)}$ and $\nu_{(C=C)}$ modes were detected at 1597 and 1514 cm^{-1}, respectively, for the free HDPPT ligand. The corresponding values for the tetranuclear $[Cu_4(DPPT)_2Cl_6]$ complex are 1549 and 1515 cm^{-1}, respectively. It is clear that the $\nu_{(C=N)}$ mode was shifted to a lower wavenumber due to complexation with the Cu(II) ion, while the $\nu_{(C=C)}$ showed almost no shift.

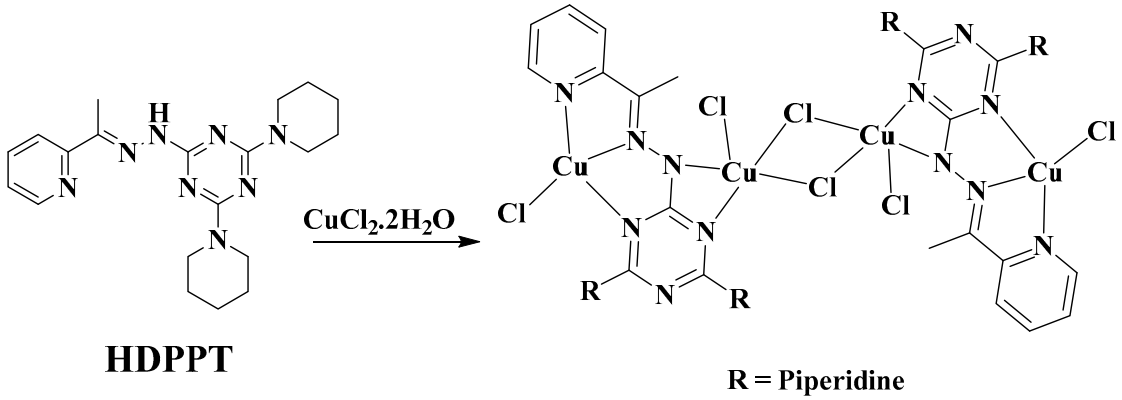

Scheme 3. Synthesis of the $[Cu_4(DPPT)_2Cl_6]$ complex.

2.2. X-ray Structure Description

The crystal structure of the newly synthesized complex approved, with no doubt, the unexpected formation of the tetranuclear Cu(II) complex of the formula $[Cu_4(DPPT)_2Cl_6]$. The asymmetric formula of this complex is half of this molecular unit, and the complex crystallized in the monoclinic crystal system, and the space group is $P2_1/c$. The unit cell parameters are a = 12.9169(9) Å, b = 19.6681(12) Å, c = 9.7335(6) Å, and β = 96.8998(19)° while z = 2. The unit cell volume is 2454.9(3) $Å^3$, and the crystal density is 1.658 Mg/m^3. The presentation of the asymmetric formula and the complete molecular structure view of the studied complex are shown in Figure 1.

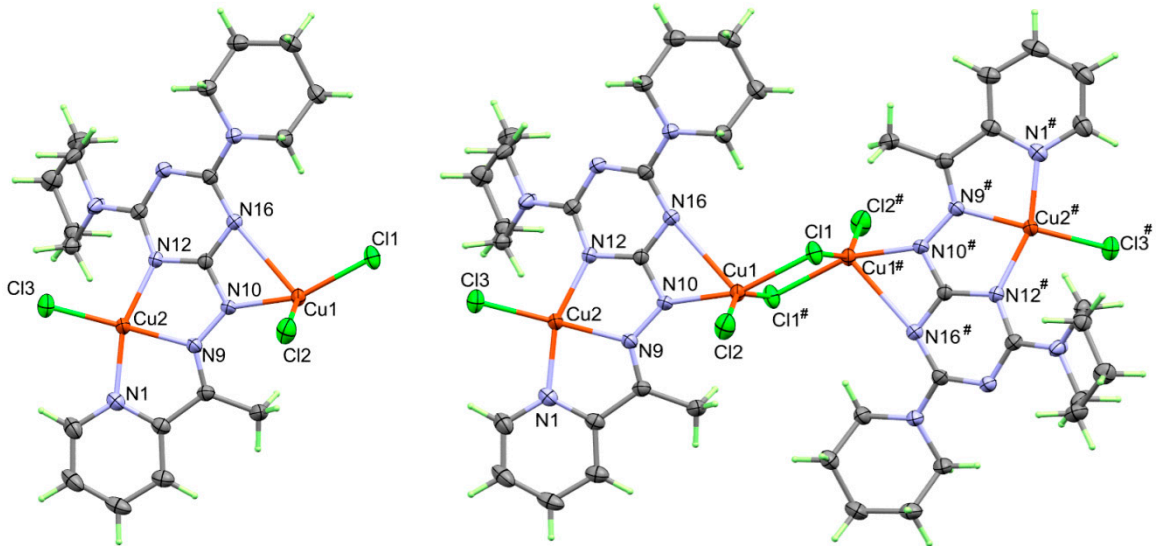

Figure 1. Asymmetric unit and molecular structures of $[Cu_4(DPPT)_2Cl_6]$. Symmetry code #: 2-X, 1-Y, 1-Z.

In the $[Cu_4(DPPT)_2Cl_6]$, there are two Cu(II) centers with different coordination environments, which are the Cu(1) and Cu(2) atomic sites. The Cu(2) atom is tetra-coordinated with the three N-atoms N1, N9 and N12 where the respective copper to nitrogen distances are 1.9899(16), 1.9539(15), and 1.9940(15) Å, while the two bite angles N1-Cu2-N9 and N12-Cu2-N9 are 80.22(6) and 79.38(6)°, respectively and the *trans* N1-Cu2-N12 angle is 156.68(6)°. The coordination sphere of the Cu(2) is completed by one chloride ligand (Cl3) where the Cu2-Cl3 distance is 2.2156(5) Å and the Cl3-Cu2-N9 angle is 159.92(5)°. The distortion of the coordination geometry around the Cu(2) site is described by τ_4 parameter using the equation $\tau_4 = -0.00709\alpha - 0.00709\beta + 2.55$ reported by Houser et al. [44]. Using the values of α and β, which are the two greatest valence angles, the τ_4 is estimated to be 0.21. Hence, the structure of the coordination environment of the Cu(2) is more close

to a distorted square planar geometry. On the other hand, the Cu(1) is pentacoordinated with CuN_2Cl_3 coordination sphere. While the organic **DPPT**$^-$ ligand anion is acting as a tridentate chelate with respect to Cu(2) site, the same ligand unit acting as a bidentate chelate for the Cu(1) site via the short Cu1-N10 (1.9702(15) Å) and the relatively long Cu1-N16 (2.643(2) Å) bonds. The bite angle N16-Cu1-N10 is 56.47(5)°. In the case of Cu(1) site, there are three coordinated chloride ions as ligands, which are the Cl2, Cl1, and Cl1# (Symm. code #: 2-X, 1-Y, 1-Z). The corresponding Cu-Cl distances are 2.2291(5), 2.2801(5), and 2.3144(5) Å. The details of the bond angles, along with the Cu-N and Cu-Cl distances, are depicted in Table 1. Based on the τ_5 parameter, which is used as a descriptor for describing the distortion in five coordinated systems, the CuN_2Cl_3 coordination sphere of the Cu(1) site is closer to the square pyramidal with τ_5 parameter of 0.15 employing Addison equation: $\tau_5 = -0.01667\alpha + 0.01667\beta$ where β and α are the N10-Cu1-Cl1 (160.21(2)°) and Cu1-Cl1-Cu2 (151.04(2)°), respectively [45]. It is worth noting that the tetranuclear formula $[Cu_4(DPPT)_2Cl_6]$ is formed by the bridged Cl1 atoms, which connect two of the asymmetric formulas via the Cu1-Cl1 bonds. Moreover, the organic ligand **DPPT**$^-$ ligand anion acts as a connector between the Cu(1) and Cu(2) sites.

Table 1. Geometric parameters (Å and °) for the coordination environment of $[Cu_4(DPPT)_2Cl_6]$.

Bond	Distance	Bond	Distance
Cu1-Cl1 #	2.3144(5)	Cu2-Cl3	2.2156(5)
Cu1-Cl1	2.2801(5)	Cu2-N1	1.9899(16)
Cu1-Cl2	2.2291(5)	Cu2-N9	1.9539(15)
Cu1-N10	1.9702(15)	Cu2-N12	1.9940(15)
Cu1-N16	2.643(2)		
Bonds	**Angle**	**Bonds**	**Angle**
Cl1-Cu1-Cl1 #	85.566(18)	N1-Cu2-Cl3	98.78(5)
Cl2-Cu1-Cl1	95.05(2)	N1-Cu2-N12	156.68(6)
Cl2-Cu1-Cl1 #	151.04(2)	N9-Cu2-Cl3	159.92(5)
N10-Cu1-Cl1 #	92.43(5)	N9-Cu2-N1	80.22(6)
N10-Cu1-Cl1	160.21(5)	N9-Cu2-N12	79.38(6)
N10-Cu1-Cl2	96.13(5)	N12-Cu2-Cl3	104.26(5)
Cu1-Cl1-Cu1 #	94.432(18)		

2-X, 1-Y, 1-Z.

The packing of the tetranuclear $[Cu_4(DPPT)_2Cl_6]$ units in the crystal is dominated by the C3-H3...Cl2 contact shown in Figure 2A. The Cl2...H3 distance is 2.64 Å, while the acceptor Cl2 to donor C3 distance is 3.549(2) Å. The view of the one-dimensional hydrogen bond polymeric structure is presented in Figure 2B.

2.3. Analysis of Molecular Packing

Crystalline materials are characterized by specific forces which hold the crystal stable and keep the molecules in a definite and unique arrangement in the three dimensions. Hirshfeld analysis is a very interesting tool to characterize these forces that hold the molecules in the crystal structure. Different Hirshfeld maps are presented in Figure 3. In the d_{norm} map of the tetranuclear $[Cu_4(DPPT)_2Cl_6]$ complex, there are several red spots characteristic for the short H...H (**A**), Cl...H (**B**), Cl...C (**C**), C...H (**D**), and N...H (**E**) interactions, which are considered evidence of the significance of these non-covalent interactions on the crystal structure stability of the tetranuclear $[Cu_4(DPPT)_2Cl_6]$ complex. The H24A...H22B (2.138 Å), Cl1...C5 (3.403 Å), Cl2...H3 (2.513 Å), C15...H20A (2.599 Å), and N16...H20A (2.572 Å) have shorter distances than the sum of the van der Waals radii sum of the two atoms sharing in these interactions (Table 2). We noted one weak C...H contact with a slightly longer interaction distance than the sum of the hydrogen and carbon van der Waals's radii sum. The C15...H4 contact has an interaction distance of 2.810 Å, while the vdWs radii sum of the H and C atoms is 2.79 Å.

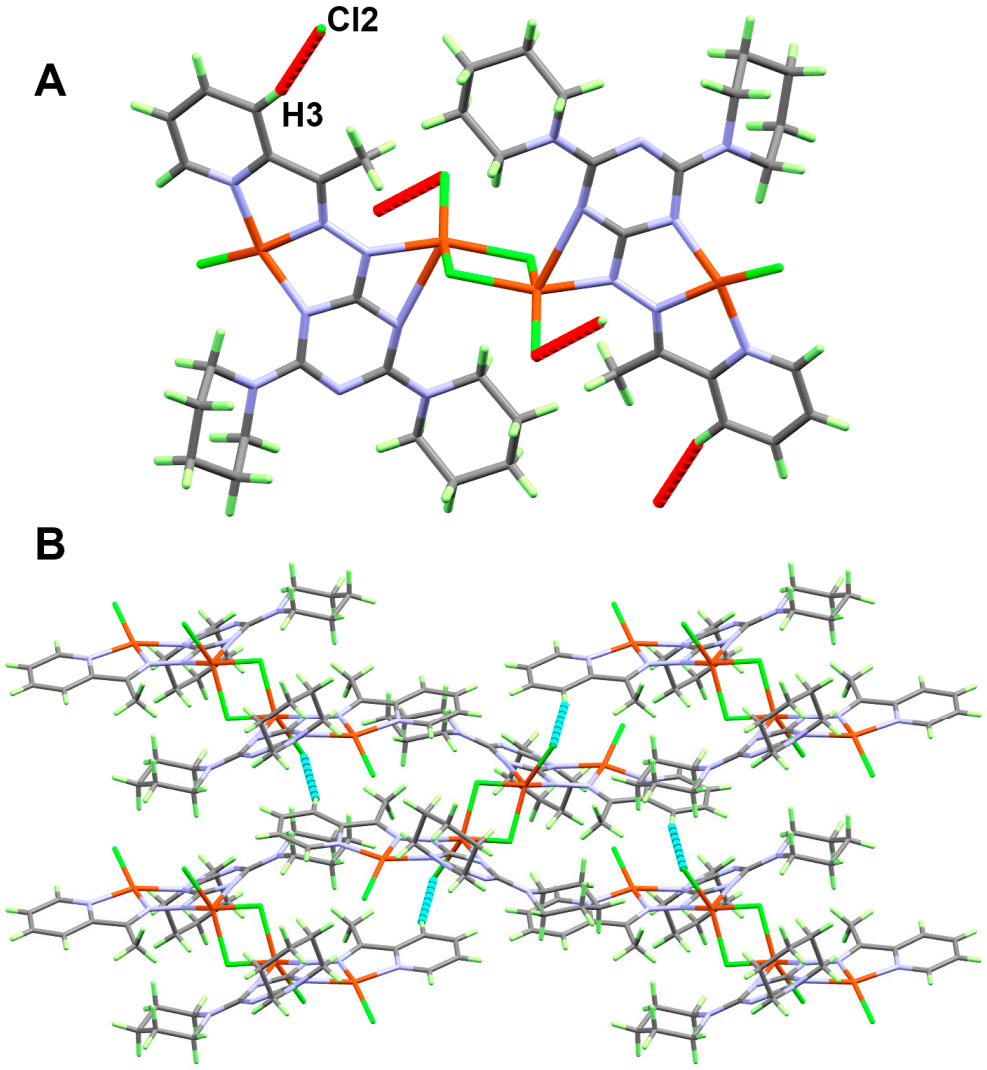

Figure 2. Intermolecular contacts (**A**) and packing view (**B**) of $[Cu_4(DPPT)_2Cl_6]$ complex.

Table 2. The short intermolecular interactions in $[Cu_4(DPPT)_2Cl_6]$ complex.

Contact	Distance
N16. . .H20A	2.572
C15. . .H20A	2.599
C15. . .H4	2.810
Cl2. . .H3	2.513
Cl1. . .C5	3.403
H24A. . .H22B	2.138

On the other hand, the fingerprint plot obtained from the Hirshfeld analysis enabled us not only to predict the significant interactions but also to estimate the percentage of each contact in the crystal structure. The H. . .H, Cl. . .H, Cl. . .C, C. . .H, and N. . .H contacts appeared as sharp spikes, revealing their importance (Figure 4). It is clear that the decomposed fingerprint plots of the H. . .H, Cl. . .H, Cl. . .C, C. . .H, and N. . .H contacts appeared as two sharp spikes. This pattern for the fingerprint plots indicates that these interactions and their reciprocals are significant and occur at short distances.

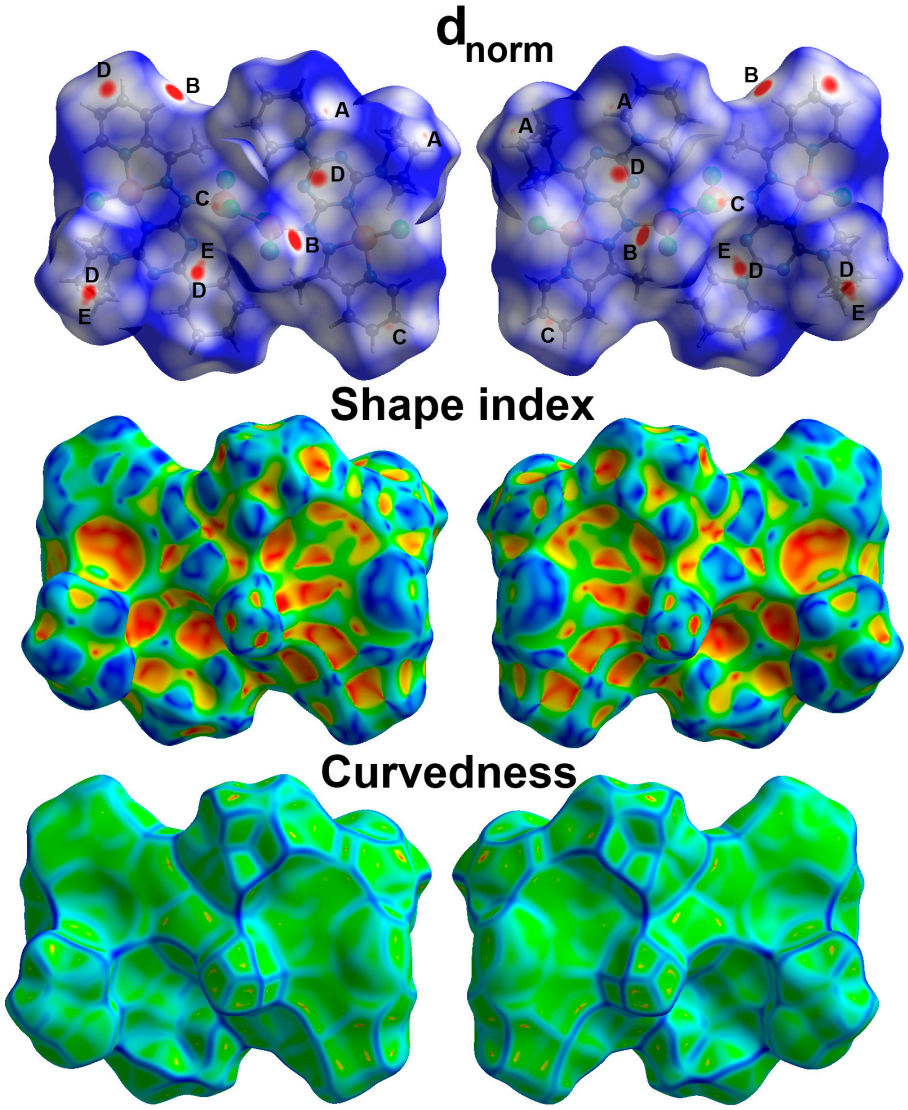

Figure 3. Hirshfeld surfaces for $[Cu_4(DPPT)_2Cl_6]$ complex.

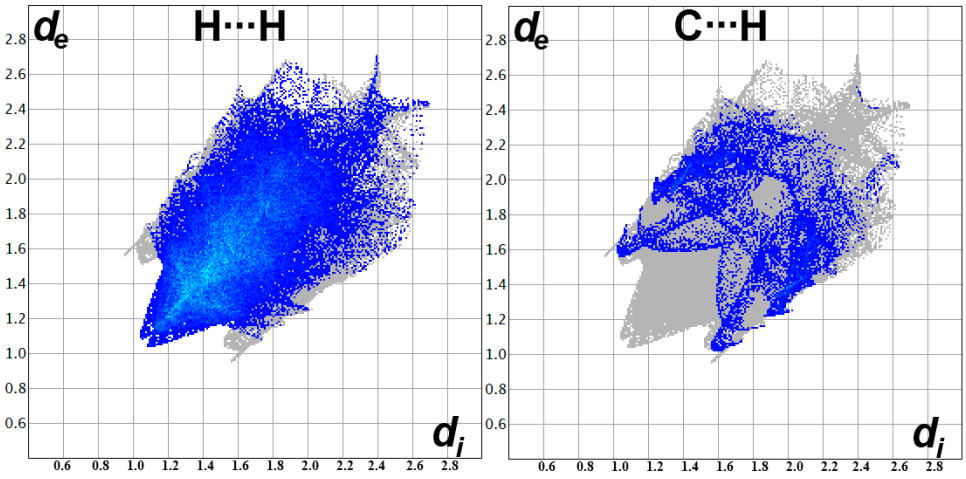

Figure 4. *Cont*.

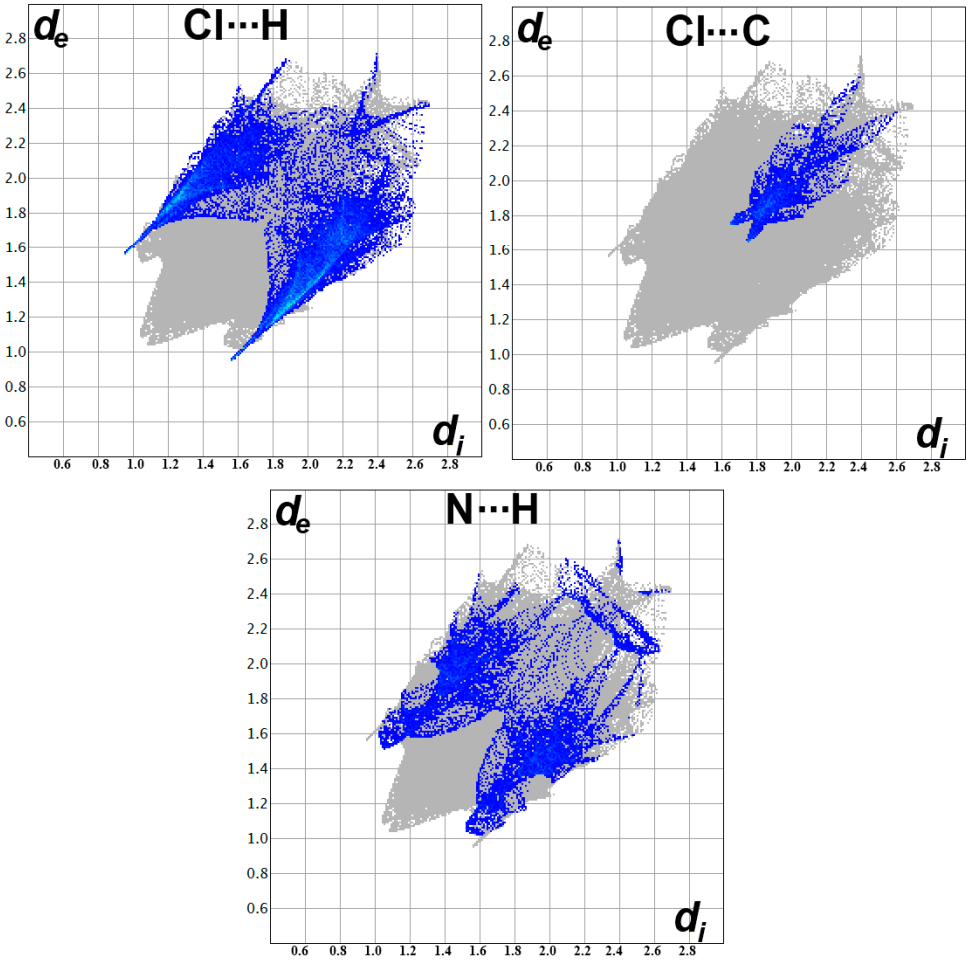

Figure 4. Fingerprint plots for the important interactions in $[Cu_4(DPPT)_2Cl_6]$.

On the other hand, the decomposition of the fingerprint plot gave the percentages of all possible interactions that could occur in the crystal structure. The presentation of all possible intermolecular contacts is shown in Figure 5. In addition, the percentages of these interactions are also presented in the same figure. The results indicated that the H. . .H and Cl. . .H interactions are the most dominant. Their percentages were estimated to be 52.8 and 19.0%, respectively. On the other hand, the percentage of the C. . .H, Cl. . .C, and N. . .H interactions are 7.7, 3.2, and 9.7%, respectively.

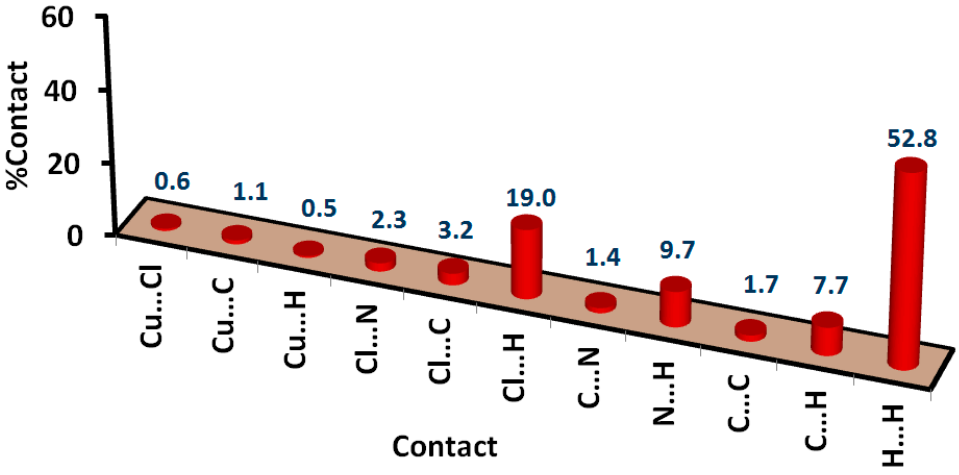

Figure 5. Intermolecular interactions in $[Cu_4(DPPT)_2Cl_6]$ complex.

In addition, other weakly contributing intermolecular contacts such as the Cu. . .Cl, Cu. . .C, Cu. . .H, Cl. . .N, and C. . .N contacts were detected in the crystal structure of the $[Cu_4(DPPT)_2Cl_6]$ complex. Their percentages were found to be 0.6, 1.1, 0.5, 2.3, and 1.4%, respectively. Their percentages are small and appear as blue or white regions in the d_{norm} map, revealing weak and less important non-covalent interactions in the molecular packing of the $[Cu_4(DPPT)_2Cl_6]$ complex.

2.4. Antimicrobial Studies

Assessment of the $[Cu_4(DPPT)_2Cl_6]$ complex and the free ligand HDPPT against some dangerous microbes was performed by detecting the inhibition zone diameters. The results are depicted in Table 3. The presence of inhibition zones with different sizes for the $[Cu_4(DPPT)_2Cl_6]$ complex indicated its broad-spectrum antimicrobial actions against the tested bacteria and fungi. In contrast, the free ligand HDPPT has no broad action against these microbes. The free ligand HDPPT is only active against *B. subtilis*. In this case, the size of the inhibition zone is only 10 mm indicating weak action against this microbe. For the rest of the studied microbes, no inhibition zones were detected for the free ligand HDPPT. In contrast, the $[Cu_4(DPPT)_2Cl_6]$ complex has zones of inhibitions with comparable sizes to the antifungal Ketoconazole and antibacterial *Gentamycin* as positive controls. The only exception from this observation is *E. coli*. For the fungal species *A. fumigatus* and *C. albicans*, the inhibition zone diameters in the case of the $[Cu_4(DPPT)_2Cl_6]$ complex are 17 and 19 mm, respectively, while for Ketoconazole, the respective values are 17 and 20 mm. Interestingly, the $[Cu_4(DPPT)_2Cl_6]$ complex has a better MIC value than Ketoconazole for *A. fumigatus,* indicating higher potency of the Cu(II) complex against this microbe. On the other hand, the $[Cu_4(DPPT)_2Cl_6]$ complex and Ketoconazole have the same MIC value for *C. albicans*. These results indicated the high antifungal activity of the $[Cu_4(DPPT)_2Cl_6]$ complex against both fungal species. On the other hand, the Ni(II) complexes of the same ligand showed comparable antifungal activity against *C. albicans* compared to the $[Cu_4(DPPT)_2Cl_6]$ complex. For the rest of the studied microbes, the Ni(II) complexes of the same ligand showed moderate antimicrobial activities compared to Ketoconazole and Gentamycin as positive controls [41] and are generally less potent than the $[Cu_4(DPPT)_2Cl_6]$ complex.

Table 3. Antimicrobial activities of the free ligand **HDPPT** [a], $[Cu_4(DPPT)_2Cl_6]$ and Ni(II)-HDPPT complexes.

Microorganism	HDPPT [b]	$[Cu_4(DPPT)_2Cl_6]$	$[Ni(HDPPT)_2](NO_3)_2$ [b]	$[Ni(HDPPT)(NO_3)Cl]$ [b]	Control
A. fumigatus	NA [c] (ND) [d]	17(78)	20 (312)	18 (312)	17(156) [e]
C. albicans	NA [c] (ND) [d]	19(312)	21 (312)	19 (312)	20(312) [e]
S. aureus	NA [c] (ND) [d]	26(4.8)	7 (5000)	8 (2500)	24(9.7) [f]
B. subtilis	10 (1250)	25(9.7)	19 (312)	22 (78)	26(4.8) [f]
E. coli	NA [c] (ND) [d]	20(78)	NA [b] (ND) [c]	NA [b] (ND) [c]	30(4.8) [f]
P. vulgaris	NA [c] (ND) [d]	22(39)	NA [b] (ND) [c]	NA [b] (ND) [c]	25(4.8) [f]

[a] Inhibition zone diameter; mm (MIC; μg/mL); [b] [41]; [c] NA: No activity; [d] ND: Not determined; [e] Ketoconazole and [f] *Gentamycin*.

Regarding the antibacterial activity, the $[Cu_4(DPPT)_2Cl_6]$ complex (26 mm) has slightly better antibacterial activity against *S. aureus* than *Gentamycin* (24 mm). The MIC value of the former is smaller than that of the latter, which reveals the higher potency of the $[Cu_4(DPPT)_2Cl_6]$ complex against *S. aureus* than *Gentamycin*. For *B. subtilis*, the inhibition zone diameter and MIC values are determined to be 25 mm and 9.7 μg/mL, respectively, which are close to *Gentamycin*. In this regard, the $[Cu_4(DPPT)_2Cl_6]$ complex has good action against the Gram-positive bacteria, which is generally comparable to *Gentamycin*. In contrast, the inhibition zone diameters for the $[Cu_4(DPPT)_2Cl_6]$ complex against *E. coli* and *P. vulgaris* are determined to be 20 and 22 mm, respectively, while for *Gentamycin*, the corresponding values are 30 and 25 mm, respectively. Moreover, the MIC values are higher for the Cu(II) complex than *Gentamycin* (Table 3). Hence, the antibacterial activity of

the $[Cu_4(DPPT)_2Cl_6]$ complex against Gram-negative bacteria is generally lower than the positive control *Gentamycin*.

3. Materials and Methods

3.1. Physical Measurements

All the chemicals were bought from Sigma-Aldrich and used without additional purifications. CHN analyses were carried out using a PerkinElmer 2400 Elemental Analyzer. The metal content was determined with the aid of a Shimadzu atomic absorption spectrophotometer (AA-7000 series, Shimadzu, Ltd., Tokyo, Japan). FTIR spectra were recorded at the Central Lab, Faculty of Science, Alexandria University, using a Bruker Tensor 37 FTIR spectrophotometer (Bruker Company, Berlin, Germany) in KBr pellets at 4000–400 cm^{-1} (Figures S1 and S2; Supplementary Materials).

3.2. Preparation of HDPPT

The **HDPPT** was prepared following the procedure reported in our previous work [41].

3.3. Synthesis of $[Cu_4(DPPT)_2Cl_6]$ Complex

Ethanolic solution of the organic ligand **HDPPT** (190.3 mg, 0.5 mmol in 10 mL) was mixed with $CuCl_2.2H_2O$ (85.2 mg, 0.5 mmol) in 5 mL ethanol. The clear mixture was left at room temperature (25 °C) for a week, dark green crystals of the $[Cu_4(DPPT)_2Cl_6]$ complex were obtained and separated from the solution by filtration. The crystals were found suitable for the X-ray single crystal structure measurement.

$[Cu_4(DPPT)_2Cl_6]$: 81.2% with respect to $CuCl_2.2H_2O$, Anal. Calc. $C_{40}H_{54}Cl_6Cu_4N_{16}$: C, 39.19; H, 4.44; N, 18.28; Cu, 20.74%. Found: C, 38.89; H, 4.32; N, 18.01; Cu, 20.55%. IR (KBr, cm^{-1}): 3061, 3002, 2973, 2855, 1549 and 1515.

3.4. X-ray Crystallography

The experimental X-ray crystallographic measurements details [46] are provided in the Supplementary Materials (Method S1). Crystal data of the $[Cu_4(DPPT)_2Cl_6]$ complex is presented in Table 4.

Table 4. Crystal data for $[Cu_4(DPPT)_2Cl_6]$ complex.

Compound	**$[Cu_4(DPPT)_2Cl_6]$**
CCDC	2287200
Empirical formula	$C_{40}H_{54}Cl_6Cu_4N_{16}$
Formula weight	1225.88
Temperature/K	173
Crystal system	monoclinic
Space group	$P2_1/c$
a/Å	12.9169(9)
b/Å	19.6681(12)
c/Å	9.7335(6)
α/°	90
β/°	96.8998(19)
γ/°	90
Volume/Å^3	2454.9(3)
Z	2
ρ_{calc}g/cm^3	1.658
μ/mm^{-1}	2.085
F(000)	1248
Crystal size/mm^3	0.09 × 0.06 × 0.04
Radiation	Mo Kα (λ = 0.71075)
2Θ range for data collection/°	3.176 to 50.73

Table 4. *Cont.*

Compound	$[Cu_4(DPPT)_2Cl_6]$
Index ranges	$-15 \leq h \leq 15$, $-23 \leq k \leq 23$, $-11 \leq l \leq 11$
Reflections collected	26,025
Independent reflections	4508 [R_{int} = 0.0212, R_{sigma} = 0.0153]
Data/restraints/parameters	4508/0/299
Goodness-of-fit on F^2	1.023
Final R indexes [$I \geq 2\sigma$ (I)]	R_1 = 0.0205, wR_2 = 0.0506
Final R indexes [all data]	R_1 = 0.0261, wR_2 = 0.0528
Largest diff. peak/hole/e Å^{-3}	0.27/−0.22

3.5. Hirshfeld Surface Analysis

The Crystal Explorer Ver. 3.1 program [47,48] was used to perform this analysis.

3.6. Antimicrobial Assay

The antibacterial activity was declared in Supplementary Materials (Method S2) [49].

4. Conclusions

In this work, the reaction product of the self-assembly of $CuCl_2.2H_2O$ and (*E*)-2,4-di(piperidin-1-yl)-6-(2-(1-(pyridin-2-yl)ethylidene)hydrazinyl)-1,3,5-triazine, (**HDPPT**) in ethanol was characterized, and its antimicrobial activity was examined. The reaction of this class of the hydrazine Schiff base ligands afforded the monomeric metal(II) complexes, unlike previous studies, an unexpected tetranuclear $[Cu_4(DPPT)_2Cl_6]$ complex was obtained. There are two differently coordinated Cu(II) sites having $Cu(1)N_2Cl_3$ and $Cu(2)N_3Cl$ coordination spheres adopting square pyramidal and square planar coordination geometries with some distortion, respectively. The supramolecular structure of the $[Cu_4(DPPT)_2Cl_6]$ complex could be described as one-dimensional hydrogen bond polymeric structure via C-H. . .Cl hydrogen bonds. Antimicrobial assessments for the $[Cu_4(DPPT)_2Cl_6]$ complex indicated promising antimicrobial activity, especially against the fungal species *A. fumigatus* and *C. albicans* as well as Gram-positive bacteria *S. aureus* and *B. subtilis*.

Supplementary Materials: The following supporting information can be downloaded at: https://www.mdpi.com/article/10.3390/inorganics11090357/s1, Figure S1: FTIR spectra of the $[Cu_4(DPPT)_2Cl_6]$ complex. Figure S2: FTIR spectra of the HDPPT. Method S1: Evaluation of antimicrobial activity [49]. Method S2: Evaluation of antimicrobial activity [49].

Author Contributions: Conceptualization, S.M.S. and A.E.-F.; methodology, H.H.A.-R., A.B., S.M.S., J.D.W. and A.M.Z.S.; software, H.H.A.-R., J.D.W. and A.M.Z.S.; validation, H.H.A.-R., A.B., S.A.A.-k. and S.M.S.; Crystallographer: J.D.W. and A.M.Z.S.; formal analysis, S.M.S. A.B., J.D.W., A.M.Z.S. and H.H.A.-R.; investigation, S.M.S., A.B., and S.A.A.-k.; resources, A.E.-F., A.B., and H.H.A.-R.; data curation, S.M.S., J.D.W., A.B., and A.M.Z.S.; writing—original draft preparation, S.M.S., A.B., H.H.A.-R., S.A.A.-k., J.D.W., A.M.Z.S. and A.E.-F.; writing—review and editing, S.M.S., A.B., H.H.A.-R., S.A.A.-k., A.E.-F., J.D.W. and A.M.Z.S.; visualization, S.M.S., J.D.W. and A.M.Z.S.; supervision, S.M.S. and A.E.-F.; project administration, S.M.S., A.E.-F. and H.H.A.-R.; funding acquisition, H.H.A.-R. All authors have read and agreed to the published version of the manuscript.

Funding: The Deputyship for Research and Innovation, "Ministry of Education", King Saud University (IFKSUOR3-188-3), Saudi Arabia.

Data Availability Statement: All data generated or analyzed during this study are included in this published article.

Acknowledgments: The authors extend their appreciation to the Deputyship for Research and Innovation, "Ministry of Education" in Saudi Arabia for funding this research (IFKSUOR3-188-3).

Conflicts of Interest: The authors declare no conflict of interest.

References

1. Huang, F.; Anslyn, E.V. Introduction: Supramolecular Chemistry. *Chem. Rev.* **2015**, *115*, 6999–7000. [CrossRef] [PubMed]
2. de Silva, A.P.; Sandanayake, K.R.A.S. Fluorescent PET (photo-induced electron transfer) sensors for alkali metal ions with improved selectivity against protons and with predictable binding constants. *J. Chem. Soc.* **1989**, *16*, 1183–1185. [CrossRef]
3. Nakahata, M.; Mori, S.; Takashima, Y.; Yamaguchi, H.; Harada, A. Self-Healing Materials Formed by Cross-Linked Polyrotaxanes with Reversible Bonds. *Chem* **2016**, *1*, 766–775. [CrossRef]
4. Wu, J.R.; Cai, L.H.; Weitz, D.A. Tough Self-Healing Elastomers by Molecular Enforced Integration of Covalent and Reversible Networks. *Adv. Mater.* **2017**, *29*, 8. [CrossRef] [PubMed]
5. Jagleniec, D.; Dobrzycki, L.; Karbarz, M. Romanski, Ion-pair induced supramolecular assembly formation for selective extraction and sensing of potassium sulfate. *J. Chem. Sci.* **2019**, *10*, 9542–9547.
6. Crane, B.C.; Barwell, N.P.; Gopal, P.; Gopichand, M.; Higgs, T.; James, T.D.; Jones, C.M.; Mackenzie, A.; Mulavisala, K.P.; Paterson, W. Advances in applied supramolecular technologies. *J. Diabetes Sci. Technol.* **2015**, *9*, 751–761. [CrossRef]
7. Williams, N.J.; Seipp, C.A.; Garrabrant, K.A.; Custelcean, R.; Holguin, E.; Keum, J.K.; Ellis, R.J.; Moyer, B.A. Surprisingly selective sulfate extraction by a simple monofunctional di(imino)guanidinium micelle-forming anion receptor. *Chem. Commun.* **2018**, *54*, 10048–10051. [CrossRef]
8. Mir, M.H.; Koh, L.L.; Tan, G.K.; Vittal, J.J. Single-Crystal to Single-Crystal Photochemical Structural Transformations of Interpenetrated 3D Coordination Polymers by [2 + 2] Cycloaddition Reactions. *Angew. Chem. Int. Ed.* **2010**, *49*, 390–393. [CrossRef]
9. Das, L.K.; Gómez-García, C.J.; Ghosh, A. Influence of the central metal ion in controlling the self-assembly and magnetic properties of 2D coordination polymers derived from $[(NiL)_2M]^{2+}$ nodes (M = Ni, Zn and Cd) (H_2L = salen-type di-Schiff base) and dicyanamide spacers. *Dalton Trans.* **2015**, *44*, 1292–1302. [CrossRef]
10. Das, L.K.; Diaz, C.; Ghosh, A. Antiferromagnetic mixed-valence Cu (I)–Cu (II) two-dimensional coordination polymers constructed by double oximato bridged Cu(II) dimers and CuISCN based one-dimensional anionic chains. *Cryst. Growth Des.* **2015**, *15*, 3939–3949. [CrossRef]
11. Yamada, T.; Otsubo, K.; Makiura, R.; Kitagawa, H. Designer coordination polymers: Dimensional crossover architectures and proton conduction. *Chem. Soc. Rev.* **2013**, *42*, 6655–6669. [CrossRef] [PubMed]
12. Li, H.; Wang, Y.; He, Y.; Xu, Z.; Zhao, X.; Han, Y. Synthesis of several novel coordination complexes: Ion exchange, magnetic and photocatalytic studies. *New J. Chem.* **2017**, *41*, 1046–1056. [CrossRef]
13. Mondal, M.; Jana, S.; Drew, M.G.; Ghosh, A. Application of two Cu (II)-azido based 1D coordination polymers in optoelectronic device: Structural characterization and experimental studies. *Polymer* **2020**, *204*, 122815. [CrossRef]
14. Zhang, Z.; Zhao, Y.; Gong, Q.; Li, Z.; Li, J. MOFs for CO_2 capture and separation from flue gas mixtures: The effect of multifunctional sites on their adsorption capacity and selectivity. *Chem. Commun.* **2013**, *49*, 653–661. [CrossRef] [PubMed]
15. Zeng, L.W.; Hu, K.Q.; Mei, L.; Li, F.Z.; Huang, Z.W.; An, S.W.; Chai, Z.F.; Shi, W.Q. Structural diversity of bipyridinium-based uranyl coordination polymers: Synthesis, characterization, and ion-exchange application. *Inorg. Chem.* **2019**, *58*, 14075–14084. [CrossRef] [PubMed]
16. Benesperi, I.; Singh, R.; Freitag, M. Copper coordination complexes for energy-relevant applications. *Energies* **2020**, *13*, 2198. [CrossRef]
17. Kardos, J.; Héja, L.; Simon, Á.; Jablonkai, I.; Kovács, R.; Jemnitz, K. Copper signalling: Causes and consequences. *Cell Commun. Signal.* **2018**, *16*, 1–22. [CrossRef]
18. Georgopoulos, G.; Roy, A.; Yonone-Lioy, M.J.; Opiekun, R.E.; Lioy, P.J. Environmental copper: Its dynamics and human exposure issues. *J. Toxicol. Environ. Health Part B Crit. Rev.* **2001**, *4*, 341–394. [CrossRef]
19. Tapia, L.; González-Agüero, M.; Cisternas, M.F.; Suazo, M.; Cambiazo, V.; Uauy, R.; González, M. Metallothionein is crucial for safe intracellular copper storage and cell survival at normal and supra-physiological exposure levels. *Biochem. J.* **2004**, *378*, 617–624. [CrossRef]
20. Neumann, W.; Gulati, A.; Nolan, E.M. Metal homeostasis in infectious disease: Recent advances in bacterial metallophores and the human metal-withholding response. *Curr. Opin. Chem. Biol.* **2017**, *37*, 10–18. [CrossRef]
21. Srivastava, S.; Panda, S.; Li, Z.; Fuhs, S.R.; Hunter, T.; Thiele, D.J.; Hubbard, S.R.; Skolnik, E.Y. Histidine phosphorylation relieves copper inhibition in the mammalian potassium channel KCa3.1. *Elife* **2016**, *5*, e16093. [CrossRef]
22. Sun, T.-S.; Ju, X.; Gao, H.-L.; Wang, T.; Thiele, D.J.; Li, J.-Y.; Wang, Z.-Y.; Ding, C. Reciprocal functions of *Cryptococcus neoformans* copper homeostasis machinery during pulmonary infection and meningoencephalitis. *Nat. Commun.* **2014**, *5*, 5550. [CrossRef]
23. Wiemann, P.; Perevitsky, A.; Lim, F.Y.; Shadkchan, Y.; Knox, B.P.; Figueora, J.A.L.; Choera, T.; Niu, M.; Steinberger, A.J.; Wüthrich, M. *Aspergillus fumigatus* copper export machinery and reactive oxygen intermediate defense counter host copper-mediated oxidative antimicrobial offense. *Cell Rep.* **2017**, *19*, 1008–1021. [CrossRef]
24. Liu, L.; Geng, X.; McDermott, J.; Shen, J.; Corbin, C.; Xuan, S.; Kim, J.; Zuo, L.; Liu, Z. Copper deficiency in the lungs of TNF-α transgenic mice. *Front. Physiol.* **2016**, *7*, 234–249. [CrossRef] [PubMed]
25. Cypryk, W.; Lorey, M.; Puustinen, A.; Nyman, T.A.; Matikainen, S. Proteomic and bioinformatic characterization of extracellular vesicles released from human macrophages upon influenza A virus infection. *J. Proteome Res.* **2017**, *16*, 217–227. [CrossRef] [PubMed]
26. Blockhuys, S.; Wittung-Stafshede, P. Roles of copper-binding proteins in breast cancer. *Int. J. Mol. Sci.* **2017**, *18*, 871. [CrossRef] [PubMed]

27. Bandmann, O.; Weiss, K.H.; Kaler, S.G. Wilson's disease and other neurological copper disorders. *Lancet Neurol.* **2015**, *14*, 103–113. [CrossRef] [PubMed]
28. Bansagi, B.; Lewis-Smith, D.; Pal, E.; Duff, J.; Griffin, H.; Pyle, A.; Müller, J.S.; Rudas, G.; Aranyi, Z.; Lochmüller, H. Phenotypic convergence of Menkes and Wilson disease. *Neurol. Genet.* **2016**, *2*, e119. [CrossRef]
29. Manto, M. Abnormal copper homeostasis: Mechanisms and roles in neurodegeneration. *Toxics* **2014**, *2*, 327–345. [CrossRef]
30. Viles, J.H. Metal ions and amyloid fiber formation in neurodegenerative diseases. Copper, zinc and iron in Alzheimer's, Parkinson's and prion diseases. *Coord. Chem. Rev.* **2012**, *256*, 2271–2284. [CrossRef]
31. He, Y.; Li, B.; O'Keeffe, M.; Chen, B. Multifunctional metal–organic frameworks constructed from meta-benzenedicarboxylate units. *Chem. Soc. Rev.* **2014**, *43*, 5618–5656. [CrossRef] [PubMed]
32. Lee, M.M.; Kim, H.Y.; Hwang, I.H.; Bae, J.M.; Kim, C.; Yo, C.H.; Kim, Y.; Kim, S.J. Cd II MOFs Constructed Using Succinate and Bipyridyl Ligands: Photoluminescence and Heterogeneous Catalytic Activity. *Bull. Korean Chem. Soc.* **2014**, *35*, 1777–1783. [CrossRef]
33. Memon, Q.S.; Memon, N.; Mallah, A.; Soomro, R.; Khuhawar, Y.M. Schiff bases as chelating reagents for metal ions analysis. *Curr. Anal. Chem.* **2014**, *10*, 393–417. [CrossRef]
34. Abu-Dief, A.M.; Mohamed, I.M.A. A review on versatile applications of transition metal complexes incorporating Schiff bases. *Beni-Seuf Univ. J. Appl.* **2015**, *4*, 119–133. [CrossRef] [PubMed]
35. Al Zoubi, W. Solvent extraction of metal ions by use of Schiff bases. *J. Coord. Chem.* **2013**, *66*, 2264–2289. [CrossRef]
36. Rezaeivala, M.; Keypour, H. Schiff base and non-Schiff base macrocyclic ligands and complexes incorporating the pyridine moiety–The first 50 years. *Coord. Chem. Rev.* **2014**, *280*, 203–253. [CrossRef]
37. Liu, X.; Hamon, J.R. Recent developments in penta-, hexa-and heptadentate Schiff base ligands and their metal complexes. *Coord. Chem. Rev.* **2019**, *389*, 94–118. [CrossRef]
38. Barakat, A.; El-Faham, A.; Haukka, M.; Al-Majid, A.M.; Soliman, S.M. s-Triazine pincer ligands: Synthesis of their metal complexes, coordination behavior, and applications. *App. Organomet. Chem.* **2021**, *35*, e6317. [CrossRef]
39. Fathalla, E.M.; Abu-Youssef, M.A.M.; Sharaf, M.M.; El-Faham, A.; Barakat, A.; Haukka, M.; Soliman, S.M. Synthesis, X-ray Structure of Two Hexa-Coordinated Ni(II) Complexes with *s*-Triazine Hydrazine Schiff Base Ligand. *Inorganics* **2023**, *11*, 222. [CrossRef]
40. Fathalla, E.M.; Abu-Youssef, M.A.M.; Sharaf, M.M.; El-Faham, A.; Barakat, A.; Badr, A.M.A.; Soliman, S.M.; Slawin, A.M.Z.; Woollins, J.D. Synthesis, Characterizations, Antitumor and Antimicrobial Evaluations of Novel Mn(II) and Cu(II) Complexes with NNN-tridentate *s*-Triazine-Schiff base Ligand. *Inorg. Chim. Acta* **2023**, *555*, 121586. [CrossRef]
41. Fathalla, E.M.; Abu-Youssef, M.A.M.; Sharaf, M.M.; El-Faham, A.; Barakat, A.; Haukka, M.; Soliman, S.M. Supramolecular Structure and Antimicrobial Activity of Ni(II) Complexes with s-Triazine/Hydrazine Type Ligand. *Inorganics* **2023**, *11*, 253. [CrossRef]
42. Soliman, S.M.; Fathalla, E.M.; Sharaf, M.M.; El-Faham, A.; Barakat, A.; Haukka, M.; Slawin, A.M.Z.; Woollins, J.D.; Abu-Youssef, M.A.M. Synthesis, Structure and Antimicrobial Activity of New Co(II) Complex with *bis*-Morpholino/Benzoimidazole-*s*-Triazine Ligand. *Inorganics* **2023**, *11*, 278. [CrossRef]
43. Soliman, S.M.; Al-Rasheed, H.H.; AL-khamis, S.A.; Haukka, M.; El-Faham, A. X-ray Structures and Hirshfeld Studies of Two Dinuclear Cd(II) Complexes with a *s*-Triazine/Pyrazolo Ligand and Pesudohalides as a Linker. *Crystals* **2023**, *13*, 1198. [CrossRef]
44. Yang, L.; Powell, D.R.; Houser, R.P. Structural variation in copper(I) complexes with pyridylmethylamide ligands: Structural analysis with a new four-coordinate geometry index, τ_4. *Dalton Trans.* **2007**, *9*, 955–964. [CrossRef]
45. Addison, A.W.; Rao, N.T.; Reedijk, J.; van Rijn, J.; Verschoor, G.C. Synthesis, structure, and spectroscopic properties of copper(II) compounds containing nitrogen–sulphur donor ligands; the crystal and molecular structure of aqua[1,7-bis(N-methylbenzimidazol-2′-yl)-2,6-dithiaheptane]copper(II) perchlorate. *J. Chem. Soc. Dalton Trans.* **1984**, *7*, 1349–1356. [CrossRef]
46. Sheldrick, G.M. A short history of SHEL. *Acta Cryst. A* **2008**, *64*, 112–122. [CrossRef]
47. Williams, G.T.; Haynes, C.J.E.; Fares, M.; Caltagirone, C.; Hiscock, J.R.; Gale, P.A. Advances in applied supramolecular technologies. *Chem. Soc. Rev.* **2021**, *50*, 2737. [CrossRef]
48. Spackman, P.R.; Turner, M.J.; McKinnon, J.J.; Wolff, S.K.; Grimwood, D.J.; Jayatilaka, D.; Spackman, M.A. Crystal Explorer: A program for Hirshfeld surface analysis, visualization and quantitative analysis of molecular crystals. *J. Appl. Crystallogr.* **2021**, *27*, 1006–1011. [CrossRef]
49. Lu, P.-L.; Liu, Y.-C.; Toh, H.-S.; Lee, Y.-L.; Liu, Y.-M.; Ho, C.-M.; Huang, C.-C.; Liu, C.-E.; Ko, W.-C.; Wang, J.-H. Epidemiology and antimicrobial susceptibility profiles of Gram-negative bacteria causing urinary tract infections in the Asia-Pacific region: 2009–2010 results from the Study for Monitoring Antimicrobial Resistance Trends (SMART). *Int. J. Antimicrob. Agents* **2012**, *40*, S37–S43. [CrossRef]